Pulse delay and propagation through subwavelength metallic slits

Paul N. Stavrinou*
Centre for Electronic Materials and Devices, The Blackett Laboratory, Imperial College London, SW7 2BX, United Kingdom

Laszlo Solymar
Department of Engineering Science, University of Oxford, Oxford OX1 3PJ, United Kingdom
(Received 29 November 2002; published 11 December 2003)

The transmission properties of a 2D metallic grating are investigated at optical wavelengths for an incident Gaussian pulse having pulse widths from 100 fs to 10 ps. The slits in the grating are subwavelength which can nevertheless allow significant transmission in the narrow wavelength regions where the so-called surface plasmon polariton (SPP) and waveguide mode resonances occur. The solution is obtained for each spectral component of the pulse by using the rigorous coupled wave approach and then the temporally varying output pulse is reconstructed by the standard method of taking an inverse Fourier transform. The delay of the pulse and the output pulse widths are determined by taking the first and second order moments of the Poynting vector with respect to time. It is shown that the time delay may be significant, as much as 256 fs for a pulse width of 200 fs for the SPP resonance but quite small (32 fs) for the waveguide mode resonance. The focus of the work is on demonstrating how the pulse delay evolves as the pulse propagates in the half-space beyond the grating. It is shown that the distance over which the time delay develops is much larger than the actual longitudinal dimension of the grating structure and it is approximately the same distance over which the stored energy and the vortices of the Poynting vector extend.

DOI: 10.1103/PhysRevE.68.066604 PACS number(s): 42.25.Bs, 42.79.Dj, 78.20.Ek, 78.67.−n

I. INTRODUCTION

It has long been known that in a linear two-port network a single frequency input wave will give rise to an output wave at the same frequency and, in general, the output wave will differ from the input wave in amplitude and phase. If the input wave is pulsed then the same considerations lead to the conclusion that the output pulse will have a somewhat different frequency spectrum and will appear with some delay. If we know the properties of the two-port network, say, the scattering coefficients and their frequency dependence, we can work out the time delay. So far this is all network theory (see e.g. [1–3]). If we wish to go further and determine the scattering coefficients in a particular case then, often, we are forced to turn to electromagnetic theory. This is particularly so at optical frequencies, the subject of the present work. Our aim is to determine, using the full apparatus of Maxwell's equations, the variation of the electric and magnetic fields for an input pulse incident upon the two-dimensional metallic grating shown in Fig. 1 with a view to find the pulse delay from field considerations [1–9]. Since the electric and magnetic fields will be available at every point we shall be able to show how the actual time delay builds up as the pulse crosses the slit and propagates into the half-space beyond. We shall then attempt to give an answer to the next relevant question that how large is the domain where the delay occurs and how it is correlated to some of the other variables calculated like the time average Poynting vector and the stored energy. Work along similar lines has been performed in the recent past where various field quantities have been studied in relation to energy flow, group velocity and pulse propagation for a variety of optical structures (see e.g. [5–9]).

The motivation for investigating this type of grating structure came from the recent experimental results of Ebbesen *et al.* [10] who showed that considerable resonant transmission may be obtained through a periodic array of subwavelength holes due to the good offices of surface plasmon polaritons (SPP). The assumption that surface plasmons are responsible for the high transmission was subsequently tested, and proved by several groups [11–14]. An earlier attempt to explain the high transmission by introducing a two-dimensional slit geometry was made by Porto *et al.* [15]. In addition to what was described as an SPP driven resonance they were able to show that for an incident *p*-polarized wave high transmission may also occur in another wavelength region (slit size being still much smaller than the wavelength) when the physical mechanism is resonant coupling at a grating thickness close to half a wavelength. Various aspects of the high transmission resonances found with these structures have been investigated (see e.g. [16–22]). In terms of field quantities, the differences between the two resonances were examined in Ref. [21] by relying on the time-average Poynting vector. In the present paper we intend to use similar techniques in the pulsed regime.

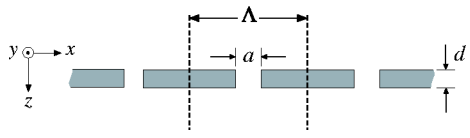

FIG. 1. A schematic representation of the metallic grating used in the present work; the structure is considered infinite in the *y* direction. Dispersive, complex permittivity values were used corresponding to gold taken from Ref. [23]. The slit width is fixed at $a = 0.5\ \mu$m and the grating period was $\Lambda = 3.5\ \mu$m.

*Email address: p.stavrinou@imperial.ac.uk

Time delay under resonant conditions in diffractive structures has been considered by Schreier *et al.* [24] for a dielectric structure by analyzing the output wave far away from the grating. They concluded that under resonance conditions a wave packet stimulates modes that are supported by the structure. Energy is coupled into these modes and coupled out with a temporal delay. Work examining the pulse delay through a metallic grating has recently been experimentally investigated by Dogariu *et al.* [25]. They measured time delays of about 7 fs when a pulse propagated through a two-dimensional array of subwavelength holes at an SPP resonance, and deduced the theoretical value from the simple model of a damped Lorentz oscillator. For the present work, pulse propagation and delay are examined at the high transmission resonances of a metallic grating comprising subwavelength slits. In Sec. II we discuss how grating diffraction for an incident pulse can be found from the solution for the stationary case and show how the pulse delay and the change in the pulse width can be obtained from first and second moments of the Poynting vector. In Sec. III we show results for the SPP resonance, in particular how the delay builds up and how it depends on the pulse width. Sec. IV shows the relatively straightforward case of the waveguide mode resonance (WGM). A short discussion analyzes the main results in Sec. V and finally conclusions are drawn in Sec. VI.

II. CALCULATION SCHEME

A. Background theory

In a previous publication [21] we investigated the steady state properties of the grating shown in Fig. 1, concentrating on high transmission zero-order resonances arising for an incident *p*-polarized plane wave. We shall now solve the same problem for the same grating parameters for an input pulse taken in the form of a carrier modulated by a Gaussian envelope. The normally incident electric field is taken in the form

$$E_x = \exp\left(-2\ln 2\frac{t^2}{\tau^2}\right)\exp i(\omega t - kz), \tag{1}$$

where t is time, z is the coordinate in the direction of propagation (see Fig. 1), ω is the carrier frequency, τ is a measure of the pulse duration (the FWHM intensity) and k is the wave number. Equation (1) provides the time variation for a single pulse which reaches the grating at $t=0$. In practice we cannot avoid turning this problem into that of a periodic set of pulses incident at a repetition frequency of $\delta\omega$ where $\delta\omega$ is the frequency interval at which the samples of the waveform are taken. Provided that the resulting temporal period between the pulses, $T=2\pi/\delta\omega$, is much larger than the pulsewidth, and the lifetime of any excited modes in the grating, the solution obtained is essentially that of a single pulse. The mathematical technique is to take the discrete Fourier transform of the incident pulse and then each spectral component (spaced $\delta\omega$ apart) can be regarded as an incident plane wave. Hence the problem reduces to that of a set of plane waves of slightly different frequencies and complex amplitudes incident upon the grating [26,27]. In the present work, the temporal period between the pulses is selected to be between $20-300\times$ the pulse width τ. The resulting spectral bandwidth of a pulse is truncated to retain envelope magnitudes which are $\geqslant 10^{-14}$ and typically involves several hundred components.

In our earlier work we obtained field distributions everywhere in space for a single incident plane wave [21]. Thus to solve the problem for pulsed incidence we only need to superimpose the solutions obtained for each spectral component. The temporal variation of the fields may then be obtained by taking an inverse Fourier transform of the full solution at each point in space. If all one wants is to determine the time delay between the input pulse and the output pulse then it is sufficient to investigate the time variation of the zero order component of the field, i.e., to disregard all the evanescent waves generated. Our aim is however to see how the time delay builds up in the immediate vicinity of the grating and, in particular, to see how large is the spatial domain which has an influence on delay. The answers to these questions lie in the properties of the evanescent waves.

B. Calculation details

The parameters of the grating (Fig. 1) are chosen to be the same as those previously examined [15,21]. The metal is taken to be gold with a dispersive complex permittivity fitted to the data provided in Ref. [23]. The grating period is $\Lambda = 3.5\ \mu$m and the width of the slit is kept fixed at $a = 0.5\ \mu$m. In the original work by Porto *et al.* [15] the spectral response for different slit widths and grating thicknesses were examined and the resulting high transmission resonances were broadly classed as arising from either SPP-like or WGM [15]. Based on this work, and following on from our previous investigation, two grating thicknesses are chosen to specifically examine the SPP ($d=0.6\ \mu$m) and WGM resonance ($d=3\ \mu$m). The resonant wavelengths are $\lambda = 3.586$ and $7.438\ \mu$m for the SPP-like and waveguide mode (WGM) resonances, respectively. Calculation of the electric and magnetic fields follows closely that of Ref. [21]. The mathematical technique used is based on rigorous coupled wave-analysis (RCWA) [28] and incorporates recent improvements to the algorithm [29,30]. We use here the same technique for each of the spectral components and from that, as outlined in the previous section, we can find all the field quantities as functions of x, z, and t.

The fields in the vicinity of the grating are given by the zero-order propagating wave and a very large number of evanescent waves (typically 100) for each of the spectral components. The number of spectral components retained varied from 100–1000 depending on the temporal width of the pulse, increasing as the pulse width decreased. From this point of view the resulting field picture is difficult to interpret. We argued in Ref. [21] that a more useful physical picture can be obtained if instead of the electric and magnetic fields (elliptically polarized in the general case hence cannot be presented as single vectors at a point in space) we rely on the time-averaged Poynting vector. In the present case we still talk about time-averaged Poynting vector but now the

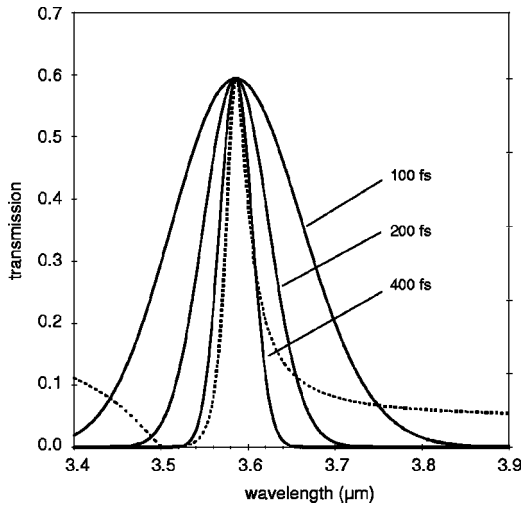

FIG. 2. The spectral representation of some Gaussian pulses, with carrier wavelength equal to the SPP resonant wavelength, superimposed with the SPP transmission spectra (dotted line).

time average means averaging over a period of the carrier frequency, i.e., we still use the complex representation $S(x,z,t)=1/2\,\mathrm{Re}[E(x,z,t)\times H^*(x,z,t)]$. The time variation due to the Gaussian envelope of the pulse remains. The spatial variation of the Poynting vector will appear in having both x and z components. The electromagnetic power may move both sideways and forward. However when our main interest is in the time delay we do not need to go into the details of lateral movement and present the passage of the pulse solely in terms of the transverse average of the z component of the Poynting vector,

$$\mathcal{S}_z(z,t)=\frac{1}{\Lambda}\int_{-\Lambda/2}^{+\Lambda/2} S_z(x,z,t)\,dx. \tag{2}$$

The expected arrival time and rms width of the pulse at a given value of z can then be obtained from the first and second moments, $\langle t\rangle$ and $\langle t^2\rangle$ as follows [8,31]:

$$\langle t(z)\rangle=\int_{-\tau}^{+\tau} t\hat{\mathcal{S}}_z(z,t)\,dt, \tag{3}$$

$$\langle t^2(z)\rangle=\int_{-\tau}^{+\tau} t^2\hat{\mathcal{S}}_z(z,t)\,dt, \tag{4}$$

where a normalized $\mathcal{S}_z(z,t)$ is assumed. Both the above measures may then be used to characterize a rms width of the pulse given by $\sigma_\tau=\sqrt{\langle t^2\rangle-\langle t\rangle^2}$. The incident pulse width as a rms measure is given by $\sigma_0=\sqrt{\tau^2/8\ln 2}$.

III. AT THE SPP RESONANCE

For plane waves incident at a single frequency the transmission as a function of wavelength is shown in Fig. 2 by dotted lines. The spectrum of a Gaussian pulse, with carrier wavelength equal to the resonant wavelength, is shown in the same figure for pulse widths of 100, 200 and 400 fs. The pulse transmission will of course depend on the width of the pulse. If the pulse is long enough the transmission will be the same as for the continuous case. As the pulse shortens the transmission declines for the spectral components away from the resonance. This is shown in Table I. For pulse widths $\geqslant 2$ ps the transmission is close to the steady state (infinite) value of 60% but the transmitted power declines to 15% for a 100 fs pulse.

TABLE I. Incident pulse widths at the SPP resonant frequency and the corresponding total diffracted transmission efficiencies along with delay and rms values measured at a distance $z=10\ \mu$m.

Pulse width		Transmission	Values at $z=10\ \mu$m	
τ (ps)	σ_0 (ps)	(%)	delay (ps)	σ_τ (ps)
0.1	0.043	15	0.212	0.225
0.2	0.085	23	0.256	0.244
0.4	0.170	35	0.303	0.293
0.6	0.254	42	0.333	0.354
0.8	0.340	47	0.352	0.423
1	0.425	50	0.365	0.493
2	0.849	56	0.402	0.874
5	2.123	59	0.415	2.144
10	4.246	59	0.418	4.257
∞		60 [a]	0.413 [b]	

[a]Obtained from the spectral response at $\lambda_{SPP}=3.586\ \mu$m.
[b]Calculated from the spectral phase response using $-\partial\phi/\partial\omega$.

To begin the temporal study, we first look at a fixed z position beyond the grating and record the time dependent power flow, averaged over a grating period [Eq. (2)]. A distance of 10 μm is chosen, which from our earlier work [21] is far enough away so both the energy density and streamlines at the SPP resonance describe basic plane wave propagation. The results for a selection of incident pulse widths are shown in Fig. 3. The overall shape of the transmitted pulses is reasonably maintained with some noticeable asymmetry found for the shorter pulses. It is also noticeable from the times when the peak power is reached that some delay has occurred, given that free-space propagation over 10 μm would amount to some 33 fs. In the case of the 100 fs pulse we have included a scaled trace of an incident pulse which has traveled the same distance in free space. Compared with the trace which has propagated through the grating, a delay can be clearly seen. (In the figure the time $t=0$ is defined as when the peak of the incident pulse reaches the start of the grating at $z=0\ \mu$m.)

To get a better indication of the transit time in the presence of the grating, the expected time for each trace is found using Eq. (3) and a delay is defined with respect to a pulse traveling the same distance through vacuum, $t_{vac}-\langle t\rangle$. The *magnitude* of delay for each pulse width considered in displayed Fig. 4 and Table I. The delay depends on duration since, for much the same reason as the duration-dependent transmitted power, in a shorter pulse only part of its spectrum is affected by the resonance. It follows that the delay is seen to increase as the incident pulse duration increases. It is noteworthy that for the shorter pulses the delay can be compa-

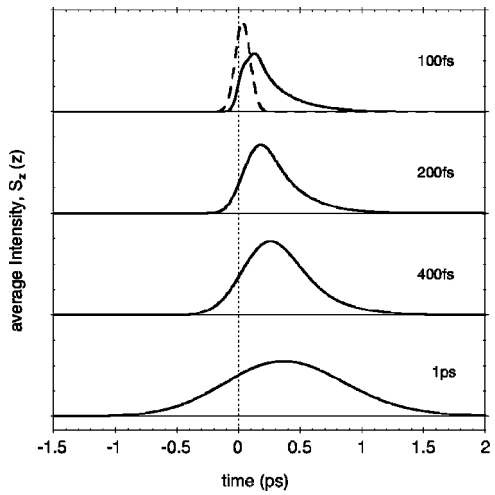

FIG. 3. Time dependent power flow for a selection of pulses recorded at a distance $z=10$ μm (9.4 μm from the grating). At $t=0$ the peak of the incident pulse reaches the grating at $z=0$ μm. Also shown in the upper plot (dashed line) is a 100 fs incident pulse (scaled by $\times 0.1$) which has traveled the same distance in free space.

rable to the pulse width, e.g., a 200 fs incident pulse is delayed by some 250 fs. For longer pulses the delay is expected to approach a limiting value dependent on $-\partial\phi/\partial\omega$ [24], where ϕ is the zero order transmitted phase response, which is straightforward to obtain numerically. The resulting delay is found to be 413 fs which is in good agreement with the limiting value suggested in Fig. 4. An approximate value for the delay can also be found from the model of a simple damped Lorentz oscillator [25] and deduced from the resonance curve. That calculation yields a value of about 400 fs.

We can of course repeat the above analysis and vary the measurement position along the z axis which will give a clearer physical picture by showing how the delay evolves. For each z position, the temporal trace [Eq. (2)] is recorded

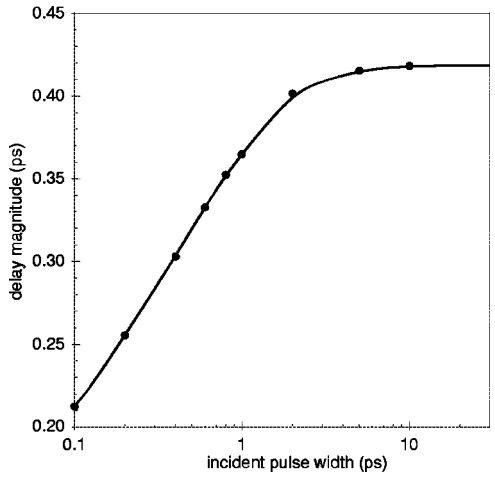

FIG. 4. The absolute values of delay, $|t_{vac}-\langle t\rangle|$, for the incident pulse widths in Table I centered at the SPP resonance and calculated at distance $z=10$ μm. (The solid line is used to guide the eye.)

and taken together form a map of $\mathcal{S}_z(z,t)$. Figure 5(a) illustrates how a delay would be represented by tracking the loci of the peak position of the pulse (or generally $\langle t\rangle$). Numerical results, displaying $\mathcal{S}_z(z,t)$ and $\langle t\rangle$ for a 400 fs pulse centered at the SPP resonance, spanning the output region from the grating are shown in Fig. 5(b). Tracking the displacement between the loci $\langle t\rangle$ and the vacuum peak, the build up of the delay is seen to continue outside the actual grating structure, up to $z\approx 2\Lambda$ away. If throughout this region the gradient of the $\langle t\rangle$ loci is considered then the instantaneous velocity of the pulse is initially around ($\approx c/20$) immediately after the grating before rising to $\approx c$ for $z\geqslant 10$ μm. At the larger distances, i.e., $z\geqslant 2\Lambda$, the delay varies very little, as shown in Fig. 5(c).

The map in Fig. 5(b) also highlights how the width of the pulse varies as it leaves the grating. Close to the grating, where the delay builds up, the local peak intensity is high and the temporal width (i.e., for a fixed z position) appears contracted compared to similar measurements taken further away. Some temporal variation of the pulse may be expected given the inevitable spectral filtering, more so for the shorter pulses. The rms width of the transmitted pulse at each z position is found and displayed along with the delay in Fig. 5(c). The spatial evolution of the width shows all activity occurs within $z\leqslant 2\Lambda$ from the grating, the same spatial extent over which the delay is established. For $z\gg 2\Lambda$ both measures show little change.

The representation of delay and rms width in this manner [Fig. 5(c)] has highlighted the significance of the environment close to the grating (i.e., $z\leqslant 2\Lambda$). Indeed when other pulse durations are considered and displayed in a similar manner, some common aspects begin to reveal themselves. In Fig. 6 we display the delay magnitude as a function of distance, whereas in Fig. 5(c), results are concerned with propagation immediately after the grating (i.e., $z\geqslant 0.6$ μm). The delay buildup for each pulse is clearly seen to continue well after the physical extent of the grating and up to $z\approx 2\Lambda$ in the propagating direction before settling to fixed values above $z>2\Lambda$. The key observation is that for all pulse widths considered (not only those shown in Fig. 6) the distance over which the delay develops appears to be the same, i.e., the spatial extent of delay evolution is *independent* of pulse duration. We also plot in Fig. 6 the variation of the stored energy, averaged over the grating period, as a function of distance for the stationary case, i.e., when a plane wave is incident at the resonant frequency. It may be seen that the region within which the energy is stored also extends to about $z\leqslant 2\Lambda$.

IV. AT THE WGM RESONANCE

To complete the study, we briefly turn to the high transmission resonance usually referred to as a waveguide mode. The appearance of these resonances can be traced to Fabry-Pérot behavior within the slits [17]. The grating thickness in Fig. 1 is taken as $d=3$ μm and the high transmission ($>80\%$) resonance occurs at 7.438 μm and as noted in Ref. [17] is longer in wavelength than $\approx 2d$. In relation to the grating period, the zero-order WGM resonance is far from

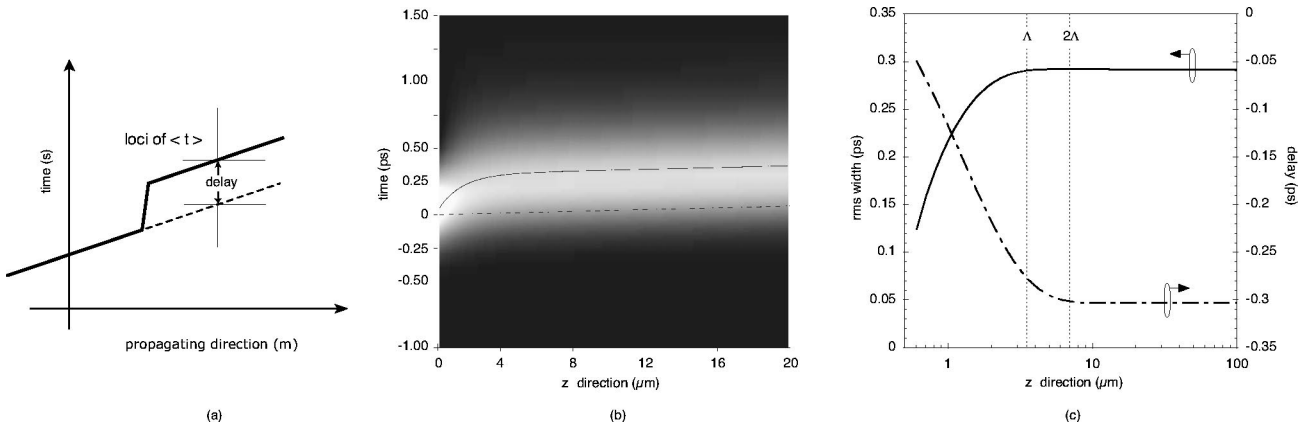

FIG. 5. Illustration of delay and numerical results for a 400 fs pulse centered at the SPP resonance. (a) A schematic showing how a transmitted delay would be represented by considering the displacement of $\langle t \rangle$ from vacuum propagation. (b) The numerical map of $\mathcal{S}_z(z,t)$ for a 400 fs pulse spanning the region immediately after the grating, the lighter regions indicate high intensity. The loci of $\langle t \rangle$ is superimposed on the map along with the equivalent measure for vacuum propagation. Tracking the displacement between these two measures illustrates the development of the delay beyond the grating (i.e., $z > 0.6\ \mu$m). (c) For a 400 fs pulse, the rms width (solid line) and delay (dash-dotted line) calculated as a function of distance beyond the grating. For both cases all activity is finished by $z \approx 2\Lambda$.

the grating cutoff and consequently the strength of evanescent field components is greatly reduced, particularly when compared with the evanescent presence for the SPP-like resonance.

Figure 7 shows the delay magnitudes for two incident pulses, 200 fs and 2 ps intensity (FWHM), with the carrier frequency set to the resonant wavelength. In both cases any development of the delay *outside* the grating is minimal, within 1 μm from the grating the delay is established. The most significant contribution to the delay is due to the propagation within the slit. A peak value of 32 fs is found from using $-\partial\phi/\partial\omega$ from the frequency response.

V. DISCUSSION

Our calculations have shown that two resonances investigated exhibit quite different behavior not only under the steady state but also under pulsed conditions. In the first case (referred to as the SPP resonance) the evanescent fields have high amplitudes whereas the evanescent amplitudes are low for the WGM resonance. We wish to emphasize that this is the major difference between the two resonances and all other properties follow from that.

Considering the SPP resonance, our earlier work had shown that due to the presence of the evanescent waves the streamlines of the Poynting vector form vortices which extend over a large distance away from the grating (about 2Λ from Fig. 2 in Ref. [21]). When the evanescent amplitudes are high the stored energy density is high as well and extends to similar distance beyond the grating (cf. Fig. 4 in Ref. [21]). In the present work we investigated a range of incident pulse widths and examined the development of a pulse *after* leaving the grating. As shown in Fig. 6 the pulse delay con-

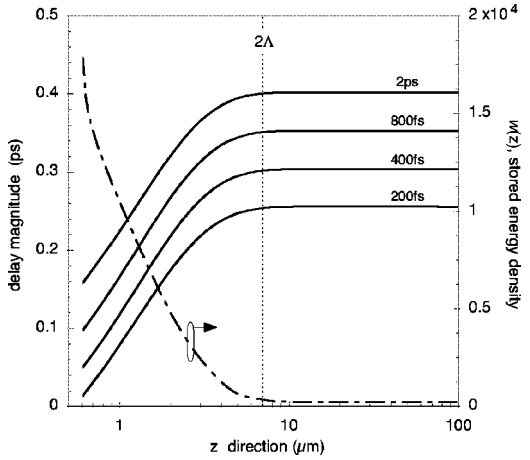

FIG. 6. Pulse delay for the SPP resonance as a function of distance beyond the grating along with the variation in stored energy density at the SPP resonance. (Solid lines) Absolute values of delay for several pulse widths. (Dash-dotted line) The steady state stored energy density evaluated at the SPP resonance and averaged over a grating period (along x).

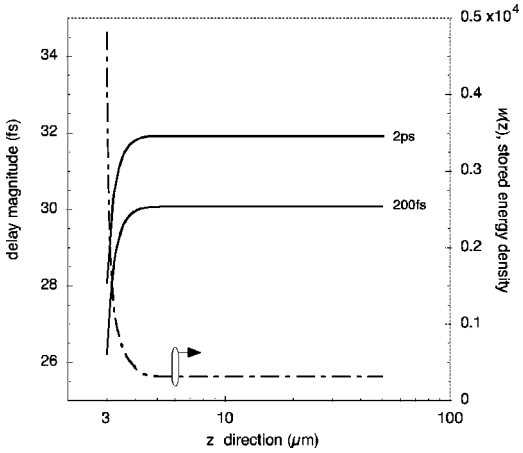

FIG. 7. Pulse delay for the WGM resonance as a function of distance beyond the grating along with the variation in stored energy density at the WGM resonance. (Solid lines) Absolute values of delay for several pulse widths. (Dash-dotted line) The steady state stored energy density averaged over a grating period (along x).

tinued to build up over the same region (i.e., over $z \leqslant 2\Lambda$).

Before we continue, it is perhaps worth making some comments about the measures we use for the calculations. The results presented in Table I and Figs. 3 and 4 are all concerned with the far field regime. The key measures used throughout were defined in Eqs. (2) and (3) and involve a spatially average Poynting vector and its temporal expected value. The use of expectation values is well established in the context of time delay [8,9]. Our use of the expected value of a spatially averaged quantity in the far field is really more for convenience than necessity. Simply tracking the temporal power flow at a single point would provide the same results. Spatial averaging becomes more useful when we turn to the near field where the field distributions and power flow is nonuniform [21] and therefore simply tracking the flow at a single point is ambiguous. However by the same token, to talk about the properties of a pulse in the near field can be equally ambiguous. What happens is that immediately after the grating the pulse breaks up, the electric and magnetic fields vary strongly, there is an additional component of the electric field and clearly there is no such thing as the direction of propagation across the unit cell. It is only when we work in the far field that we can properly speak of the reappearance of the pulse. This does not mean however that there is neither rhyme nor reason for the buildup of the delay. Once we concentrate on average quantities over the unit cell the general trend becomes clear. Definitions of time delay in the near-field different from ours are of course possible. Nevertheless useful features of our approach include a continuous measure from the near to the far field, and the quantities involved, such as the total power across a surface or the total stored energy, are those appearing in Poynting's theorem.

The correlation between $\mathcal{W}$, the total stored energy, and delay has long been known for lossless networks [1–3]. For our situation we consider a region beyond the grating as a lossless network. The time required ($\mathcal{T}$) for a pulse of energy to enter and leave the region is the average stored energy (W) per unit incident power ($\mathcal{P}$) and may be written as

$$\mathcal{T} = \frac{\mathcal{W}}{\mathcal{P}}. \tag{5}$$

For the stationary wave the total stored energy is

$$\mathcal{W} = \int_0^z w(z)\,dz, \tag{6}$$

where $w(z)$ is the average (over x) stored energy per unit volume. Hence the time delay is related to the derivative of the total stored energy density and, indeed, this is borne out by Fig. 6. Where w is high the rate of change of delay is high as well. When w declines to zero the delay no longer changes. A similar line of reasoning may be used for the WGM resonance. As already noted, the evanescent field amplitudes in this case are low and consequently the stored energy outside the grating structure is low. Any further development of the delay, above that which occurs within the structure, is expected to be minimal and this is indeed what Fig. 7 suggests.

Our picture so far has used the steady state stored energy, evaluated at the SPP resonant frequency, which appears to yield good correlation with the spatial variation of delay. However, it is also seen from Table I, Figs. 4 and 6 that the delay can be dependent on pulse width. To properly account for this the temporal variation of the stored energy density under pulsed conditions would be required. We believe there will still be a strong correlation. Further investigations along these lines are currently underway.

VI. CONCLUSION

We have investigated the delay a pulse suffers while passing through a 2D metallic grating comprising subwavelength slits at carrier frequencies corresponding to two kinds of high transmission resonances, commonly referred to as surface plasmon polariton and waveguide mode resonances. We have shown for the SPP resonance the greater part of the pulse delay occurs not only within the grating structure but continues to develop beyond the grating up to a distance of twice the grating period. Conversely for the WGM resonance, the delay is essentially established inside the grating structure. The contrasting behavior has been linked to the total stored energy and the evanescent field amplitudes present in each case. Since the analysis has been based on field quantities the conclusions reached are very likely to have wider implications within the general field of subwavelength diffracting structures, such as photonic crystal structures.

ACKNOWLEDGMENT

The authors would like to thank Professor G. Parry for many useful discussions and encouragement. This work is supported within the Ultrafast Photonics Consortium (UPC) financed from the U.K. Engineering Research Council (EPSRC).

[1] C. Montgomery, R. Dicke, and E.M. Purcell, *Principles of Microwave Circuits* (McGraw-Hill, New York, 1948).

[2] P. Penfield, Jr., R. Spence, and S. Duinker, *Tellegen's Theorem and Electrical Networks* (M.I.T. Press, Cambridge, MA, 1970).

[3] R. Collin, *Foundations for Microwave Engineers*, 2nd ed. (McGraw-Hill, New York, 1992).

[4] C. Ernst, V. Postoyalko, and N.G. Khan, IEEE Trans. Microwave Theory Tech. **49**, 192 (2001).

[5] M. Scalora, J.P. Dowling, A.S. Manka, C.M. Bowden, and J.W. Haus, Phys. Rev. A **52**, 726 (1995).

[6] M. Scalora, R.J. Flynn, S.B. Reinhardt, R.L. Fork, M.J. Bloemer, M.D. Tocci, C. Bowden, H.S. Ledbetter, J.M. Benedickson, J.P. Dowling, and R.P. Leavitt, Phys. Rev. E **54**, R1078 (1996).

[7] G. D'Aguanno, M. Centini, M. Scalora, C. Sibilia, M.J. Bloemer, C.M. Bowden, J.W. Haus, and M. Bertolotti, Phys. Rev. E **63**, 036610 (2001).
[8] J. Peatross, S.A. Glasgow, and M. Ware, Phys. Rev. Lett. **84**, 2370 (2000).
[9] S. Glasgow, M. Ware, and J. Peatross, Phys. Rev. E **64**, 046610 (2001).
[10] T. Ebbesen, H. Lezec, H. Ghaemi, T. Thio, and P. Wolff, Nature (London) **391**, 667 (1998).
[11] E. Popov, M. Neviére, S. Enoch, and R. Reinisch, Phys. Rev. B **62**, 16100 (2000).
[12] L. Salomon, F. Grillot, A. Zayats, and F. de Fornel, Phys. Rev. Lett. **86**, 1110 (2001).
[13] L. Martín-Moreno, F.J. García-Vidal, J. Lezec, K.M. Pellerin, T. Thio, J.B. Pendry, and T.W. Ebbesen, Phys. Rev. Lett. **86**, 1114 (2001).
[14] R. Wannemacher, Opt. Commun. **195**, 107 (2001).
[15] J. Porto, F.J. García-Vidal, and J.B. Pendry, Phys. Rev. Lett. **83**, 2845 (1999).
[16] W.-C. Tan, T. Preist, and J. Sambles, Phys. Rev. B **62**, 11134 (2000).
[17] Y. Takakura, Phys. Rev. Lett. **86**, 5601 (2001).
[18] M.M.J. Treacy, Appl. Phys. Lett. **75**, 606 (1999).
[19] Q. Cao and P. Lalanne, Phys. Rev. Lett. **88**, 057403 (2002).
[20] S. Collin, F. Pardo, R. Teissier, and J.L. Pelouard, Phys. Rev. B **63**, 033107 (2001).
[21] P.N. Stavrinou and L. Solymar, Opt. Commun. **206**, 217 (2002).
[22] A. Barbara, P. Quémerias, E. Bustarret, and T. Lopez-Rios, Phys. Rev. B **66**, 161403 (2002).
[23] *Handbook of Optical Constants of Solids*, edited by E. Palik (Academic, Orlando, 1985).
[24] F. Schreier, M. Schmitz, and O. Bryngdahl, Opt. Lett. **23**, 1337 (1998).
[25] A. Dogariu, T. Thio, L.J. Wang, T.W. Ebbesen, and H.J. Lezec, Opt. Lett. **26**, 450 (2001).
[26] H. Ichikawa, J. Opt. Soc. Am. A **16**, 299 (1999).
[27] W. Nakagawa, R-C. Tyan, P.-C. Sun, F. Yu, and Y. Fainman, J. Opt. Soc. Am. A **18**, 1072 (2001).
[28] M. Moharam, E. Grann, D. Pommet, and T. Gaylord, J. Opt. Soc. Am. A **12**, 1068 (1995).
[29] L. Li, J. Opt. Soc. Am. **13**, 1870 (1996).
[30] P. Lalanne and M. Jurek, J. Mod. Opt. **45**, 1357 (1998).
[31] R. Bracewell, *The Fourier Transform and Applications*, 2nd ed. (McGraw-Hill, New York, 1986).